JOURNAL OF GEOPHYSICAL RESEARCH, VOL. 106, NO. D24, PAGES 34221–34233, DECEMBER 27, 2001

A preliminary three-dimensional global model study of atmospheric methyl chloride distributions

J. M. Lee-Taylor and G. P. Brasseur[1]
National Center for Atmospheric Research, Boulder, Colorado, USA

Y. Yokouchi
National Institute for Environmental Studies, Tsukuba, Ibaraki, Japan

Abstract. A global three-dimensional atmospheric model of methyl chloride (CH_3Cl) is presented. When incorporating known terrestrial and oceanic source terms, the tropospheric budget of CH_3Cl is unbalanced. We show that a reduction in the atmospheric CH_3Cl loss rate could account for the net budget discrepancy but fails to reproduce the observed latitudinal distribution. We find that observed mixing ratios and latitudinal distributions can be reproduced by addition of a tropical terrestrial CH_3Cl source of 2330–2430 Gg yr^{-1} combined with a 50% reduction in the southeastern Asian biomass burning contribution. This is equivalent to a net source of 3800–3900 Gg yr^{-1}, slightly higher than previously estimated. The magnitude of additional emissions required to match observations is sensitive to their latitudinal distribution. We successfully simulate tropical land-based observations best when the added source is increased at the coasts relative to inland areas. Mixing ratios at remote sites are relatively insensitive to the finer details of the source parameterization.

1. Introduction

Methyl chloride (CH_3Cl), the most abundant natural organic chlorine compound in the troposphere, is also the major naturally produced contributor to stratospheric chlorine. CH_3Cl constituted about 15% of stratospheric total organic chlorine in 1991–1992 [*Schauffler et al.*, 1993] and is expected to increase in relative importance in the future as anthropogenic chlorine abundances decrease in response to recent emission regulations [e.g., *Montzka et al.*, 1999a]. Natural emission and destruction rates of CH_3Cl may vary in response to future climatic changes in temperature and atmospheric water vapor. Understanding of the tropospheric budget is desirable, therefore, to allow assessment of potential impacts on stratospheric chemistry resulting from global change.

The mean mixing ratio of CH_3Cl in the remote troposphere is usually measured at about 550 parts per trillion by volume (pptv) [*Koppmann et al*, 1993; *Moore et al.*, 1996; *Yokouchi et al*, 2000]. Values reported according to the Rasmussen scale are consistently about 10% higher, at around 600 pptv [e.g., *Khalil and Rasmussen*, 1999], probably due to a calibration discrepancy [*Khalil et al.*, 1999]. All observations and flux quantities originating from the Rasmussen calibration scale and quoted in this work are rescaled to a mean atmospheric CH_3Cl mixing ratio of 550 pptv, for consistency.

The latitudinal distribution of CH_3Cl is different from that of many other halocarbons, especially those with mainly anthropogenic sources. The interhemispheric difference reverses on a seasonal basis, with higher mixing ratios in the winter/spring hemisphere [*Khalil and Rasmussen*, 1999; *Montzka et al.*, 1999b], and stronger seasonal cycle amplitude in the Northern Hemisphere than in the Southern. Annual mean distributions are fairly symmetrical about the equator, where mixing ratios are 50–60 pptv higher than at middle to high latitudes [*Yokouchi et al.*, 2000]. *Khalil and Rasmussen* [1999] suggest small temporal trends at some locations, though calibration issues currently prevent confirmation of such trends from other data [*Kurylo et al*, 1999]. Of more significance is a long-term 5–10% increase in CH_3Cl mixing ratios since the early 1900s, shown in firn air analyses [*Butler et al.*, 1999].

Considerable effort has been devoted to assessing the tropospheric budget of CH_3Cl under the Reactive Chlorine Emissions Inventory (RCEI) project [*Graedel and Keene*, 1999; *Keene et al.*, 1999; *Khalil et al.*, 1999; *Lobert et al.*, 1999; *McCulloch et al.*, 1999], a component of the International Global Atmospheric Chemistry Programme (IGAC) Global Emissions Inventory Activity (GEIA). However, the budget remains unbalanced. RCEI-identified sources, which total about 1880 Gg yr^{-1} [*Keene et al.*, 1999], can only account for approximately one half of the observed atmospheric burden and calculated chemical loss. *Khalil and Rasmussen* [1999] estimated a net global CH_3Cl source of 3400 Gg yr^{-1} (rescaled from their quoted value of 3700 Gg yr^{-1}) in a simple inverse study of remote atmospheric observations. They concluded that about 85% of emissions take place in the tropics and subtropics. Observations of elevated mixing ratios in landward air relative to maritime air suggest that tropical coastal land and/or vegetation produce strong fluxes [*Yokouchi et al.*, 2000].

Since the publication of the RCEI inventories, ecosystem-specific field studies have identified several new and potentially significant sources of CH_3Cl. Substantial emissions have been observed from salt marshes [*Rhew et al.*, 2000; *Varner et al.*, 2000] and, to a lesser extent, from inland peat bogs [*Varner et al.*, 1999; *Dimmer et al.*, 2001]. Rice cultivation also contributes to CH_3Cl emissions [*Redeker et al.*, 2000]. Global extrapolation gives an estimate of 233 Gg yr^{-1} from these three sources, albeit with a wide range of uncertainty.

In this study we investigate the CH_3Cl budget using the three-dimensional chemistry-transport Intermediate Model of Global Evolution of Species (IMAGES) [*Müller and Brasseur*, 1995], described briefly in section 2. Section 3 lists the known sources

[1]Now at Max Planck Institute for Meteorology, Hamburg, Germany.

Paper number 2001JD900209.
0148-0227/01/2001JD900209$09.00

Table 1. The "Known" CH_3Cl Budget as Derived From Literature Relationships (See Text) and Implemented in Our Model

Budget Term	Gigagrams per Year (Uncertainty)	Gigagrams Cl per Year	Reference
Biomass burning A	910 (650–1120)	640	*Lobert et al.* [1999]
Biomass burning B[a]	733	515	see text
Net oceanic	477 (40–950)	335	after *Khalil et al* [1999]
Salt marshes	170 (65–440)	120	*Rhew et al.* [1999]
Industry/incineration	162 (30–294)	114	*McCulloch et al.* [1999]
Fungal	128 (35–385)	90	after *Watling and Harper* [1998] and *Khalil et al.* [1999]
Wetlands	48 (no range given)	34	*Varner et al.* [1999]
Soil sink	−256 (highly uncertain)	−180	*Keene et al.* [1999]; after *Khalil and Rasmussen* [1999]
Total (A)[b]	1639 (1020–3189)	1153	

[a] Alternate to source "pyrogenic A," adopted for later simulations in the present study.
[b] Net uncertainty excludes uncertainty in soil sink and wetland source.

and sinks of CH_3Cl. These were distributed globally and, where warranted, seasonally, to assess the current budget shortfall. Section 4 discusses the sensitivity of the modeled CH_3Cl distribution to uncertainties in the atmospheric oxidation rate of CH_3Cl by OH. In section 5 we explore the addition of a series of hypothetical new sources based on the information of *Yokouchi et al.* [2000] and *Khalil and Rasmussen* [1999] and compare the resulting CH_3Cl distributions with observational data. Conclusions are presented in section 6.

2. Model Description

IMAGES [*Müller and Brasseur*, 1995] is a global three-dimensional (3-D) chemical transport model of the lower atmosphere with 5° × 5° horizontal resolution and 25 vertical σ-coordinate levels, extending to 50 mbar (approximately 20 km altitude). Tracer transport is driven by monthly averaged winds from a European Centre for Medium-Range Weather Forecasts (ECMWF) analysis. Wind variability is parameterized as a mixing process, with diffusion coefficients calculated from the ECMWF variances. Deep convection in cumulonimbus clouds, planetary boundary layer mixing, and other enviromental variables are also parameterized as monthly averages. Photodissociation rates are interpolated from a look-up table. Surface gas emissions are based on the inventory of *Müller* [1992], updated as per *Müller and Brasseur* [1995] and *Granier et al.* [1996]. Subsequent model refinements are listed by *Lee-Taylor et al.* [1998].

The major chemical loss mechanism for CH_3Cl is reaction with OH in the troposphere. Our modeled OH distribution yields global lifetimes for methyl chloroform and methane of 4.4 and 8.7 years, consistent with the values of 4.6 ± 0.3 and 8.9 ± 0.6 years calculated by *Prinn et al.* [1995]. Tropospheric photolysis of CH_3Cl is insignificant. Rate expressions included in the model for photolysis of and OH reaction with CH_3Cl are taken from *DeMore et al.* [1997]. The model is initialized with a globally uniform CH_3Cl mixing ratio and run with a 1-day time step for 4–6 years. Annual changes in the CH_3Cl mixing ratio are less than ±1% in the final year. The calculated CH_3Cl global lifetime is 1.3 years, identical to that quoted by *Khalil* [1999].

3. Known Methyl Chloride Budget Terms

Our estimates of the known surface fluxes of methyl chloride are largely based upon the Reactive Chlorine Emissions Inventory (RCEI) publications by *Keene et al.* [1999], *Khalil et al.* [1999], *Lobert et al.* [1999], and *McCulloch et al.* [1999]. Each of these papers synthesized the work of many previous investigators, giving a comprehensive description of the then known sources of reactive chlorine-containing gases and of methyl chloride in particular. More recent studies of specific sources are listed here in section 3.6.

CH_3Cl budget terms are reported in the literature in terms of masses of both CH_3Cl and Cl. Here we report CH_3Cl flux amounts in units of Gg yr^{-1} (1 Gg = 1 kT = 0.001 Tg). We include conversions to units of Gg Cl yr^{-1}, where appropriate, for comparison with the RCEI literature. In general, we use in our model the quoted net flux and distribution if a budget term is based on data compilations. Where budget terms arise from stated relationships to environmental variables, we recalculate the net flux using the environmental databases linked to our model. Where the budget term arises from extrapolation but the global relationship is not quoted in the literature, we use available environmental parameters to distribute the given net flux. Values originating from the Rasmussen calibration scale are rescaled to a mean atmospheric CH_3Cl mixing ratio of 550 pptv. The known surface sources and sinks used in our model are summarized in Table 1 and Figure 1.

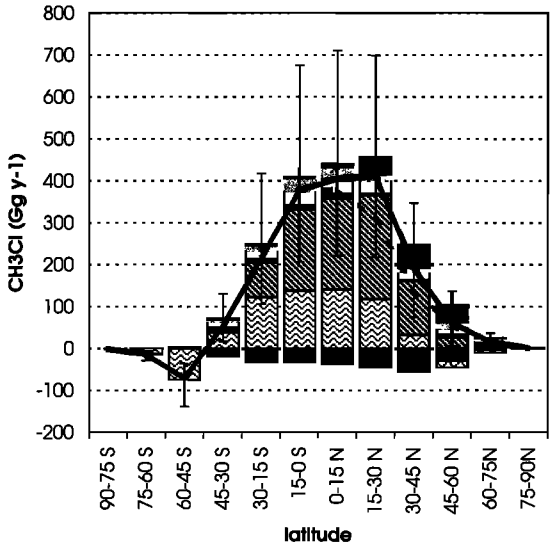

Figure 1. Fifteen-degree-binned latitudinal distribution of the known sources and sinks of CH_3Cl. Legend is as follows: darker shaded bars, industry/incineration source; lighter shaded bars, fungal source; open bars with squares, salt marsh/mangal source; solid bars,wetland source; diagonally striped bars, biomass burning source; wavy patterned bars, oceanic flux; solid bars with open dots, soil sink. Net flux is shown as follows: solid curve, fluxes as presented in the literature (case A); dashed curve, net flux with reduced Asian biomass burning (case B). Error bars show the sum of the stated uncertainties for all terms in case A except the soil sink and wetland source.

3.1. Biomass Burning

Biomass burning is the largest known source of CH_3Cl to the atmosphere. *Lobert et al.* [1999] estimated this source as 910 (650–1120) Gg yr^{-1} (640 Gg Cl yr^{-1}), based on a wide-ranging data compilation. Emissions are concentrated in tropical regions, especially India and Southeast Asia. Nine burning categories were defined, including savanna, scrubland, and forest fires, agricultural waste and fuel wood burning, and fires due to forest clearance. The analysis considered emission ratios of CH_3Cl to both CO and CO_2.

We imposed seasonality on the annual modeled biomass burning flux of *Lobert et al.* [1999] by scaling CH_3Cl emissions at each location to the seasonal cycle of CO_2 emissions [*Granier et al.*, 1996], without regard to type of burning involved. CO_2 is emitted primarily from the fires' flaming phase, whereas CH_3Cl, like CO, is emitted primarily from the smoldering phase [e.g., *Manö and Andreae*, 1994] and is therefore favored by moister conditions. Our treatment assumed implicitly that the monthly mean relative strengths of flaming and smoldering fires remained constant in any one grid box.

Our seasonal climatology of biomass burning emissions shows a bimodal pattern, with emissions from northern equatorial Africa, Southeast Asia, and India peaking in April and May, and those from South America (Amazon region) and southern Africa peaking in October and November. A net CH_3Cl flux from biomass burning of 910 Gg yr^{-1} was included in our model for OH sensitivity runs and for the initial investigations of the potential missing source (scenario A, solid curve in Figure 1). For later simulations, in order to reduce the modeled interhemispheric gradient, CH_3Cl fluxes from southern and eastern Asia were halved. This reduced the net biomass burning CH_3Cl flux to 733 Gg yr^{-1} (scenario B, dashed curve in Figure 1). The reduction is within the stated bounds of uncertainty, which are especially great in this region since the emissions factors relating burning-derived carbon emissions and CH_3Cl release from domestic fuel use in India and rice straw burning in China are particularly poorly quantified (J. Lobert, personal communication, 2000).

3.2. Air-Sea Exchange

The ocean is the second largest known source for methyl chloride. *Khalil et al* [1999] estimated an annual global net flux of 440 Gg yr^{-1} (310 Gg Cl yr^{-1}) from in situ observations. They also made a larger estimate of 655 Gg yr^{-1} (460 Gg Cl yr^{-1}), using a National Oceanic and Atmospheric Administration Climate Monitoring and Diagnostics Laboratory (NOAA-CMDL) proxy relationship between CH_3Cl saturation anomaly and sea surface temperature (SST,°C), which they combined with lowest-model-layer winds from the National Centers for Atmospheric Research (NCAR) Community Climate Model (CCM3) [*Kiehl et al.*, 1996]. Both estimates were quoted relative to a mean atmospheric concentration of 540 pptv. Uncertainties were stated as being about a factor of 2 in each direction, owing mainly to differences between published transfer velocity relationships.

We recalculated the CH_3Cl oceanic flux, using the NOAA-CMDL proxy relationship [*Khalil et al.*, 1999] with monthly mean observed 10-m wind speeds averaged over the 4-year period 1985–1988 from the National Centers for Environmental Prediction (NCEP)-NCAR reanalysis [*Kalnay et al.*, 1996]. SST was taken from the climatology of *Shea et al.* [1990, 1992]. Transfer velocities of CH_3Cl across the air-sea interface were calculated using the version of *Wanninkhof*'s [1992] equation appropriate for long-term average wind speed;

$$k_{1\mathrm{CH3Cl}}(\mathrm{m\,s^{-1}}) = 0.39V^2(Sc_{\mathrm{CH3Cl}}/660)^{-1/2}/3.6 \times 10^5, \quad (1)$$

where V is the monthly mean wind speed (m s^{-1}) at 10 m above sea level. Sc_{CH3Cl} is the Schmidt number of methyl chloride (the kinematic viscosity of seawater divided by the viscosity of CH_3Cl, a unitless quantity) as defined by *Khalil and Rasmussen* [1999]:

$$Sc_{\mathrm{CH3Cl}} = 2385[1 - 0.065(\mathrm{SST}) + 0.002043(\mathrm{SST})^2 - 2.6e - 5(\mathrm{SST})^3]. \quad (2)$$

Our resulting global oceanic net flux estimate was 477 Gg yr^{-1} (335 Gg Cl yr^{-1}), for a uniform tropospheric mixing ratio of 550 pptv. This compares favorably with the 440 Gg yr^{-1} extrapolated by *Khalil et al.* [1999] from in situ cruise observations and is 27% lower than their modeled result, which was used in the budget summary paper of *Keene et al.* [1999].

3.3. Industry/Incineration Missions

Methyl chloride is also released as a by-product of coal combustion and waste incineration, with global emissions of 75 ± 70 and 32 ± 23 Gg Cl yr^{-1}, respectively [*McCulloch et al.*, 1999]. The same authors estimated chemical industry emissions at 7 Gg Cl yr^{-1}, giving a total industry/incineration source of 162 Gg CH_3Cl yr^{-1} (114 ± 93 Gg Cl yr^{-1}). The distribution is comparatively well constrained by data. Sources are greatest in the eastern United States, Britain, eastern Europe, India, and China, with only around 11 Gg yr^{-1} from the Southern Hemisphere (see Figure 1). Emissions from coal combustion for domestic and electricity generation purposes are likely somewhat seasonal; however, we applied the industry/incineration flux to the model as an annual rate.

3.4. Fungal Emissions

The potential flux to the atmosphere of methyl chloride as a by-product of the fungal decay of wood has been estimated as 156 (43–470) Gg yr^{-1} (110 Gg Cl yr^{-1}) [*Watling and Harper*, 1998; *Khalil et al.*, 1999]. No global distribution has yet been presented, due possibly to the lack of field data. For the present study we estimated a global annual flux distribution following the methods of the previous investigators and of *Lee-Taylor and Holland* [2000]. The flux is parameterized thus:

$$F = \sum_{i=1}^{t} (D_i[Cl^-]_i\, f_{\mathrm{nat},i}\, k_i), \quad (3)$$

where, for each model cell i, F is the flux (mg Cl yr^{-1}), D is the annual decomposition rate (kg dry matter yr^{-1}) assessed for preagricultural (i.e., natural) conditions [*Matthews*, 1983; *Matthews*, 1997], $[Cl^-]$ is the content of Cl^- (mg kg^{-1} dry matter) in wood [*Khalil et al.*, 1999], and f_{nat} is the fraction of the grid cell occupied by natural vegetation [*Matthews*, 1983]. The net fractional efficiency of conversion by fungi of Cl^- in litter to CH_3Cl, k, combines expressions for the availability of wood for fungal attack, the relative abundances of fungus species grouped according to halide-releasing ability, and the CH_3Cl release efficiencies of these fungi [*Watling and Harper*, 1998; *Khalil et al.*, 1999; *Lee-Taylor and Holland*, 2000].

We estimated and adopted a total annual CH_3Cl fungal emission flux of 128 Gg yr^{-1} (90 Gg Cl yr^{-1}). Emissions are concentrated in the tropical rainforest regions but also occur in the boreal forests in this representation. Seasonality is not considered. Our flux estimate is 80% of that of *Khalil et al.* [1999], since we used a different assessment of global woody decomposition. As all other factors are drawn from their work, the range of uncertainty associated with our CH_3Cl flux estimate is proportional to theirs, at 35–385 Gg yr^{-1}.

3.5. Soil Sink

Keene et al. [1999] quote a global soil sink for CH_3Cl of 256 Gg yr^{-1} (180 Gg Cl yr^{-1}), based on the work of *Khalil and Rasmussen* [1999]. No estimate is available of the soil uptake distribution, although it is believed to be widespread. Consequently, the size of

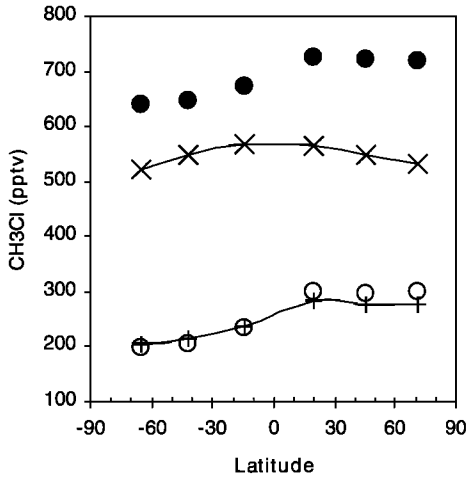

Figure 2. CH_3Cl mixing ratios calculated using control conditions (plus signs and thin curve), OH reaction rates at the lower limit of stated uncertainty (solid circles), and inverted OH distribution (open circles). Reference data (crosses) are adapted from *Khalil and Rasmussen* [1999]. Values are four-season (January, April, July, October) mean mixing ratios at locations South Pole (90°S), Cape Grim (42°S, 145°E), Samoa (14°S, 171°W), Hawaii (19°N, 153°W, sea level), Cape Meares (46°N, 124°W), and Barrow (71°N, 157°W). Modeled clean-air mixing ratios for Cape Grim (CGO) are assessed in the 5° × 5° oceanic grid box 50–600 km directly south of CGO's actual location, to avoid including the effects of land-based emissions from Tasmania, which is downwind of but in the same grid cell as CGO.

this sink is also very uncertain, and *Khalil and Rasmussen* [1999] omit it from their budget assessment. More recently, *Keppler et al.* [2000] presented evidence for abiotic production of CH_3Cl within the soil profile but made no global extrapolation.

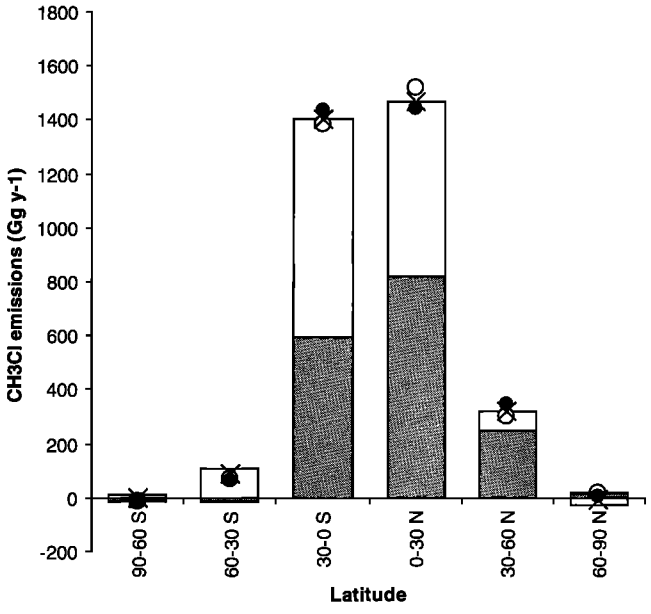

Figure 3. "First guess" CH_3Cl source parameterization, by 30° bins. Crosses represent the net source calculated by *Khalil and Rasmussen* [1999] adjusted to a 550 pptv mean background CH_3Cl mixing ratio. The shaded areas represent the net known source (section 3); the unshaded areas represent the implied missing source. Symbols show our parameterized net source, including pseudobiogenic source with threefold coastal enhancement (open circles, run 1C) and without (solid circles, run 1U).

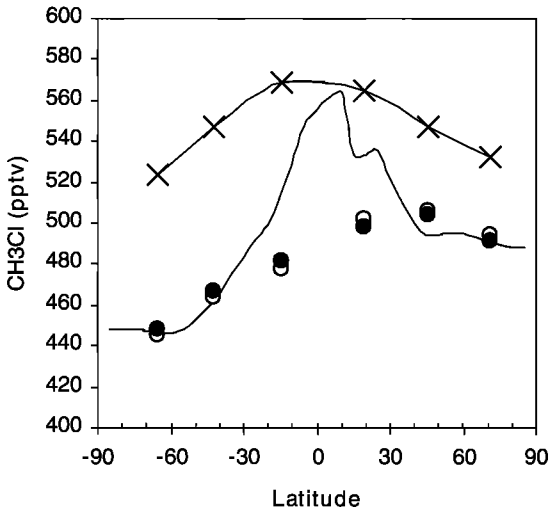

Figure 4. Model results from the first guess pseudobiogenic source. Solid circles indicate run 1U; solid curve represents run 1U zonal mean; open circles indicate run 1C; and crosses indicate reference data as described in Figure 2 caption.

We parameterized soil uptake of CH_3Cl by assuming proportionality to a methyl bromide (CH_3Br) soil sink extrapolation (*Lee-Taylor et al.* [1998], from observations of *Shorter et al.* [1995] and a microbial activity/soil temperature relationship [*Cleveland et al.*, 1993; *Holland et al.*, 1995]). There is, admittedly, no evidence for or against such an assumption. This parameterization results in Northern and Southern Hemisphere sinks of 171 and 85 Gg yr^{-1}, totaling 256 Gg yr^{-1}.

3.6. Newly Identified Terrestrial Sources

Emissions of CH_3Cl from two California salt marshes were extrapolated over an estimated global coastal marsh area of 3.8 × 10^5 km^2, giving a total flux of 170 (65–440) Gg yr^{-1} [*Rhew et al.*, 2000]. Later measurements [*Varner et al.*, 2000] found comparable emissions rates from eastern United States salt marshes. We are not aware of any global database of coastal marshes, and therefore we modeled the flux of *Rhew et al.* [2000] according to the distribution of coastal marsh regions (temperate and tropical) depicted by *Chapman* [1997]. We confined emissions to the growing season, defined by a minimum monthly mean surface temperature of 6°C. The resulting distribution gives 104 Gg yr^{-1} from the Northern Hemisphere and 66 Gg yr^{-1} from the Southern (Figure 1).

Flux measurements from inland peat bog ecosystems led *Dimmer et al.* [2001] to estimate a 5.5 (0.9–43.4) Gg yr^{-1} global source from peatlands, while fluxes from all freshwater wetlands worldwide are estimated as 48 Gg yr^{-1} [*Varner et al.*, 1999] and 35 Gg yr^{-1} [*Dimmer et al.*, 2001]. Emission rates used for the global wetland flux estimates differ by a factor of 2: The closer agreement of the totals arises from extrapolations over differing assessments of global wetland area. We distributed the 48 Gg yr^{-1} flux of *Varner et al.* [1999] using the wetland database of *Matthews and Fung* [1987], which gives the larger area. Emissions were restricted to the growing season, as defined above.

Emissions of CH_3Cl from flooded rice fields have also been identified recently [*Redeker et al.*, 2000], with fluxes evolving whether or not plants are present. Extrapolation gives a tentative global flux of 5.8 Gg yr^{-1}. We did not include this flux in our study.

4. Sensitivity of the Modeled CH_3Cl Distribution to Reaction With OH

In their synopsis of the CH_3Cl budget, *Keene et al.* [1999] suggested that the stated uncertainty in the temperature depend-

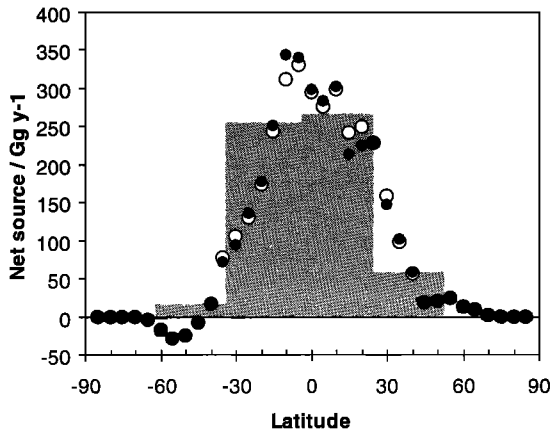

Figure 5. First guess CH_3Cl net source parameterization, zonal totals by 5° bins. Shaded region indicates estimate of *Khalil and Rasmussen* [1999]; solid circles indicate run 1U; and open circles indicate run 1C.

ence of the OH + CH_3Cl reaction rate constant presented by *DeMore et al.* [1997] could account for much of the discrepancy in the global CH_3Cl budget. The lower limit of uncertainty is equivalent to a reduction of the rate by factors of 1.2 and 2 at 298 and 257 K, respectively. To test the response of the modeled budget to these changes, we used the scenario A known sources and sinks (see section 3) in two model runs: a control run, with the stated OH reaction rate, and a run using the lower limit of the rate. Results are presented in Figure 2, with, for comparison, the rescaled four-season mean of the observations after Figure 7c of *Khalil and Rasmussen* [1999] (crosses). We do not attempt to assess model response to uncertainty associated with the known sources since it is unclear how this uncertainty should be distributed. However, increasing each source to the maximum of its uncertainty range (see Table 1) increases the sum of the known sources by about 50%.

The imbalance in the known global CH_3Cl budget led to modeled mixing ratios in the control run (plus signs, Figure 2) that were about one half of observed values. Decreasing the OH reaction rate to the limit of its uncertainty range yielded a latitude-weighted mean mixing ratio of 691 pptv, greater than observed values. However, both sets of model results show a pronounced interhemispheric gradient, a feature which is absent from the observations. The gradient is 63 pptv, or 25%, in the control run and 73 pptv (11%) in the run with the decreased OH rate. We have confidence in the model's latitudinal representations of OH chemistry and transport, due to good reproduction of the observed latitudinal distribution of methane [*Müller and Brasseur*, 1995]. Therefore we attribute the modeled CH_3Cl interhemispheric gradient to the higher emissions from the Northern Hemisphere than the Southern in the known budget (Figure 1). We conclude that if OH reaction rate uncertainty is to be invoked to assist in CH_3Cl budget closure, a significant unidentified source must also be added at higher latitudes in the Southern Hemisphere, to remove the modeled interhemispheric gradient. It is difficult to imagine how such a southern source might be produced, as oceanic observations, which are reasonably well constrained [*Khalil et al.*, 1999], already suggest a net sink at higher southern latitudes. It is more likely that the OH reaction rates quoted by *DeMore et al.* [1997] are close to the actual rates and that a "missing" land-based or atmospheric source of similar magnitude to the sum of the known sources [*Keene et al.*, 1999], and with a significant southern component, remains to be elucidated.

Equatorial asymmetries in tracer distribution may also be produced by north-south asymmetries in the distribution of sinks for that tracer. We assessed the sensitivity of the modeled interhemispheric gradient to the model OH distribution by inverting it such that northern and southern OH values were swapped and the seasonal cycle was advanced by 6 months. In this case (Figure 2, open circles) the CH_3Cl interhemispheric difference increased to 93 pptv, or 36% of the mean. This result seems counterintuitive at first, since the model (in the control run) has 15% more tropospheric OH in the Southern Hemisphere than in the Northern. However, a detailed examination of the control case [see *Müller and Brasseur*, 1995, Figure 27] actually shows more OH in the boundary layer of the Northern Hemisphere than of the Southern, in agreement with *Spivakovsky et al.* [2000, Figure 6]. Latitudinal inversion of the model OH distribution thus increases the boundary layer lifetime and mixing ratio of CH_3Cl in the Northern Hemisphere and reduces both quantities in the Southern, enhancing the interhemispheric difference. This result suggests that the interhemispheric difference in CH_3Cl is robust for our model and the known emissions, and reinforces the conclusion that the missing portion of the CH_3Cl budget should be biased toward the Southern Hemisphere.

5. An Hypothetical Tropical Source

This section describes a series of model runs incorporating different estimated "missing source" distributions. Comparisons of model results with atmospheric observations illustrate the sensitivity of the modeled mixing ratio distribution to source input parameters.

5.1. Parameterization of the Additional Source

The origin of the additional missing source is a subject of current investigation. Tropical measurements show close correlations between local enhancements of CH_3Cl and of biogenic compounds emitted by terrestrial plants [*Yokouchi et al.*, 2000]. It is unknown whether this reflects direct biogenic emission of CH_3Cl, atmospheric transformations of other biogenic species [e.g., *Keene et al.*, 1999], or some other combination of processes. We assumed in this study that terrestrial plants have a significant role in CH_3Cl production. Foliar emissions of several volatile organic compounds (VOCs) have been related to foliar density, temperature, and available light [*Guenther et*

Table 2. Summary of Section 5.3 Run Parameters and Results

Run[a]	Pseudobiogenic Source, Gg yr^{-1}	N/S Ratio of Added Source	Burden, Tg	Six-Site Mean Mixing Ratio	Annual Global Mixing Ratio
3800-w	2330	0.80	4.8	551	578
3800-w-coastal	2330	1.04	4.9	555	581
3900-h	2430	0.79	4.9	562	589
4000-w	2530	0.80	5.0	578	606
4100-h	2630	0.79	5.1	588	617

[a] Letters "w" and "h" mean pseudobiogenic source emitted where annual mean $T \geq 288$ and 293 K, respectively. "Coastal" means pseudobiogenic emissions restricted to within 2° of the coast.

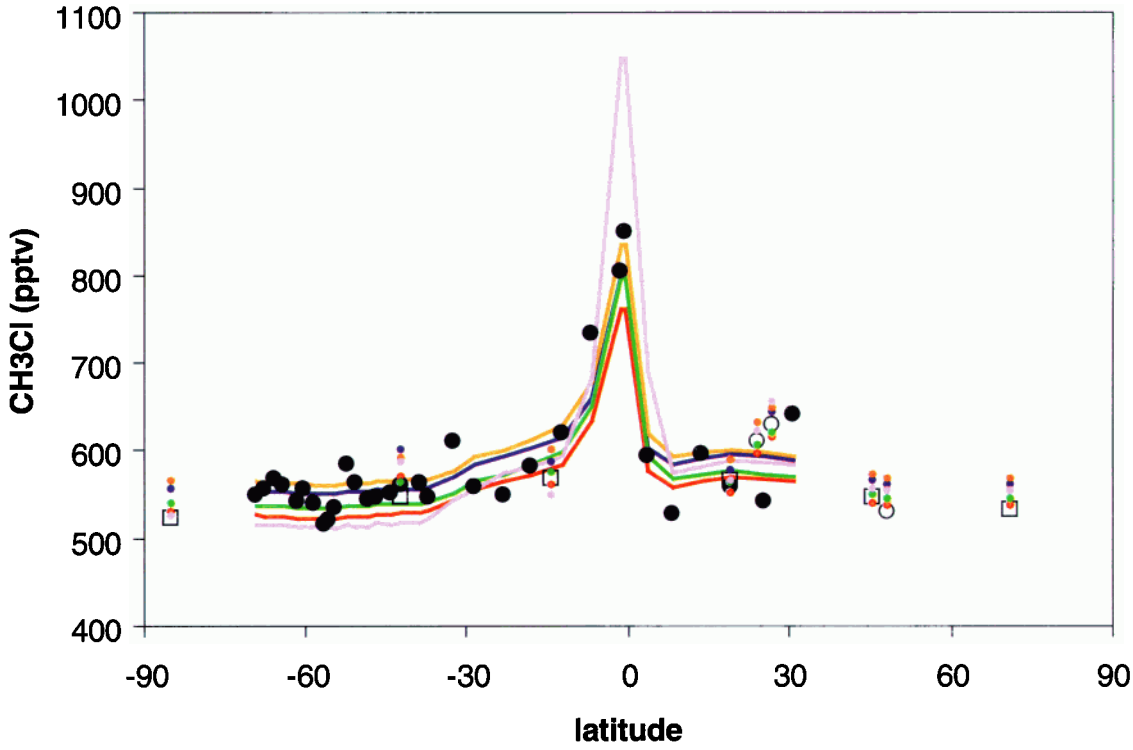

Plate 1. Comparisons between Pacific data and model results. Black represents data: solid circles represent instantaneous shipborne measurements [*Yokouchi et al.*, 2000]; open circles represent short-term means from locations listed in text [*Yokouchi et al.*, 2000]; open squares represent long-term means from stations as in Figure 2 [*Khalil and Rasmussen*, 1999]. Colors represent model results: red, run 3800-w; green, run 3900-h; blue, run 4000-w; orange, run 4100-h; purple, run 3800-w-coastal; dots represent annual mean results at measurement sites; curves represent model results on ship track.

al., 1995]. Thus we distributed our CH_3Cl fluxes proportionally to satellite-derived leaf area index (LAI) [*Guenther et al.*, 1999] and parameterized seasonal variation in some simulations using an empirical relationship between temperature and isoprene

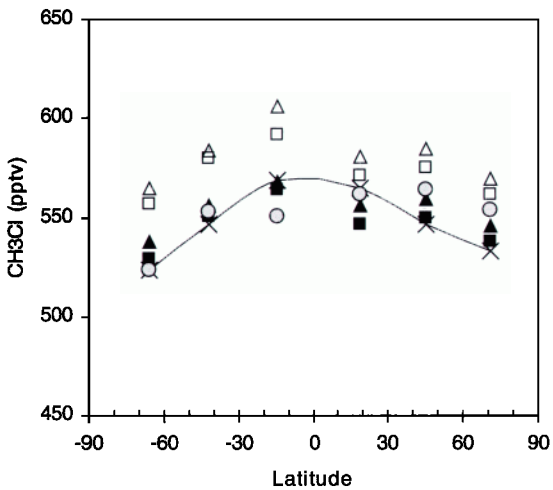

Figure 6. Summary of model results at six remote sites. Data treatment is as for Figure 2. Solid squares indicate run 3800-w; solid triangles indicate run 3900-h; open squares indicate run 4000-w; open triangles indicate run 4100-h; shaded circles indicate run 3800-w-coastal; and crosses indicate reference data. The vertical scale is comparable to that of Figure 4.

foliar emissions [*Guenther et al.*, 1995]. Northern and southern limits of the source were constrained by annual mean surface temperature, implying that vegetation in cooler climate regions would not contribute significantly. One simulation used only fluxes from within 2° of the coast. We refer to the parameterized "missing" or "additional" tropical source as "the pseudobiogenic source."

For each simulation we defined a "target" latitudinal pattern for the pseudobiogenic source based on comparisons of previous model output to atmospheric observations. This was possible because modeled CH_3Cl mixing ratios are a near-linear combination of contributions from the different sources. We varied the parameters governing the new source estimate to match the target source distribution. Cutoff temperatures below 285 K gave too great a proportion of emissions from the Northern Hemisphere, due to the larger land surface there. The relatively coarse 5° × 5° resolution of our model cannot adequately represent the contribution of small islands, so parameterizing emissions from only coasts also unavoidably increased the Northern Hemispheric contribution to the additional tropical flux.

5.2. Incorporation of Previous Source Estimates Into the 3-D Model

Figure 3 shows our "first guess" net source, derived from the 30° binned net source estimated by *Khalil and Rasmussen* [1999] with a simple zonal mean inverse model. The scenario A known sources described in section 3 were subtracted in each bin from the estimated net source, giving an implied global missing source of 1625 Gg yr^{-1}. Modeled mixing ratios resulting from the addition of this source (Figure 4) were significantly lower than observed mixing ratios and showed a distinct interhemispheric difference.

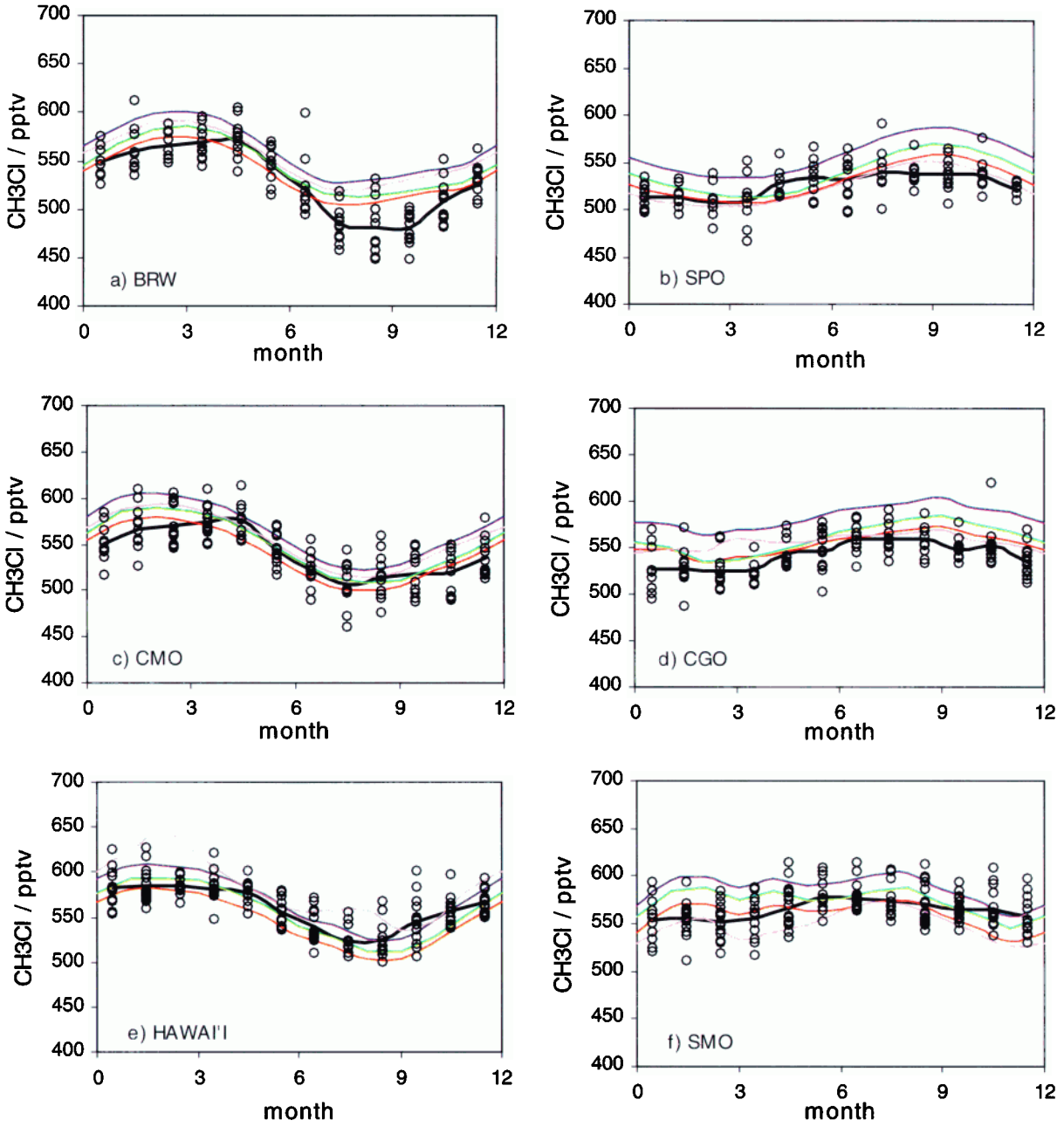

Plate 2. Comparisons of model results with monthly mean long-term observations at (a) Barrow; (b) South Pole; (c) Cape Meares; (d) Cape Grim; (e) Cape, Kumukahi, Hawaii; and (f) Samoa. Circles indicate data of *Khalil and Rasmussen* [1999]; black curves indicate mean of the observations; red curves indicate run 3800-w; green curves indicate run 3900-h; blue curves indicate run 4000-w; purple curves indicate run 3800-w-coastal.

At least two factors contributed to the modeled mixing ratio shortfall. First, the original global source estimate was made from clean-air observations [*Khalil and Rasmussen*, 1999]. However, measurements [*Yokouchi et al.*, 2000] show CH_3Cl mixing ratios to be zonally inhomogeneous, which leads to a greater atmospheric burden than that obtained by global extrapolation of clean-air mixing ratios alone. Our 3-D model showed elevated mixing ratios over source regions, and zonal mean mixing ratios (Figure 4, solid curve) that often exceed remote site values at the same latitude. Latitudinally weighted annual mean model mixing ratios were 489 pptv when based on the six remote sites and were 505 pptv globally.

A second reason for the shortfall is the difference in resolution between our simulation and that of *Khalil and Rasmussen* [1999]. Although not apparent from Figure 3, our source parameterizations had emissions maxima nearer to the equator within each 30° latitude band than did the binned source of *Khalil and Rasmussen* [1999] (Figure 5). Atmospheric destruction rates of CH_3Cl vary in response to temperature and OH abundance. Therefore CH_3Cl emitted nearer the equator has a shorter atmospheric lifetime relative to that released at higher latitudes, leading to lower modeled mixing ratios overall.

The simulated interhemispheric difference in CH_3Cl arises mainly from the northern bias of modeled CH_3Cl emissions,

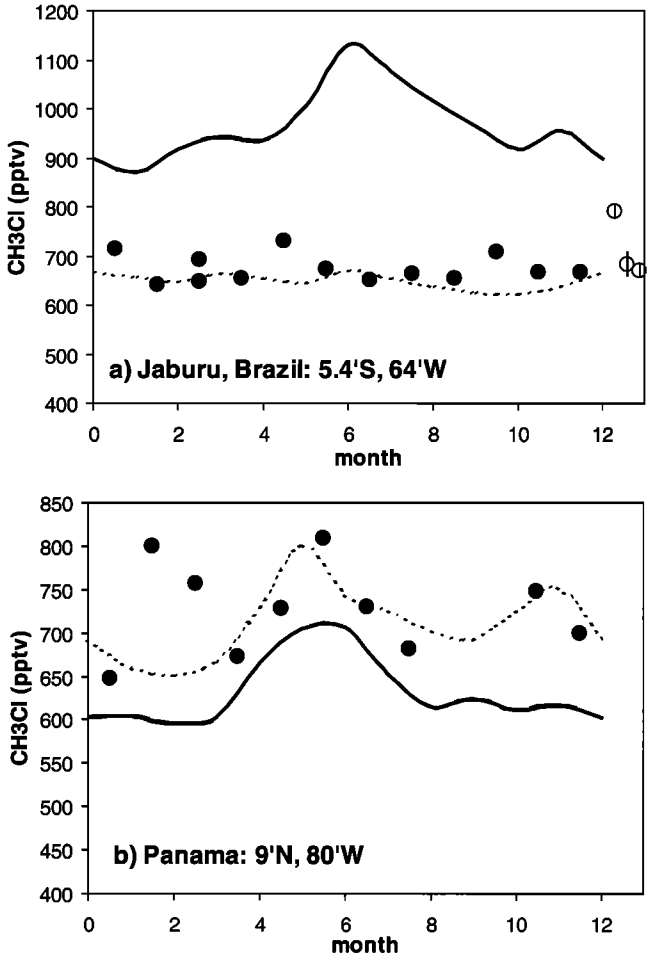

Figure 7. Response of model results to coastal enhancement of the pseudobiogenic source at (a) Jaburu (5°S, 64°W) and (b) Panama (9°N, 80°W). Solid curves indicate run 3800-w; dotted curves indicate run 3800-w-coastal. Solid symbols represent data accredited in the text. Open symbols in Figure 7a are the annual mean values from three other Brazilian sites [*Khalil and Rasmussen*, 1999].

especially the asymmetry of the biomass burning contribution (Figure 1). It was difficult to parameterize a pseudobiogenic source that could compensate for this bias. Since the biomass burning flux comprises many different, regional terms [*Lobert et al.*, 1999], it may be considered on a regional basis, whereas the next largest known source, the oceanic flux, is based on a globally applied relationship. We found that a 50% reduction in the Southeast Asian biomass burning source (scenario B; see Figure 1 and section 3.1) reduced the annual mean interhemispheric difference assessed between Barrow (BRW) and South Pole (SPO) and modeled from known budget components alone, by about one third, to 48 pptv. Simulations discussed in the remainder of this paper incorporate the reduced Asian biomass burning source.

5.3. New Estimates of the Pseudobiogenic CH_3Cl Source

A series of new estimates of the size and distribution of the pseudobiogenic source was made by optimizing model results to match CH_3Cl measurements from the remote Pacific region. We estimated the contribution of the unidentified source by subtracting from the measurements the mixing ratios attributable to the known sources (that is, the results of our scenario B control run). We then assessed the gross differences between the residual mixing ratios for the real unidentified source and for our simulated pseudobiogenic source and adjusted the next pseudobiogenic source estimate accordingly. Seasonality was applied to the pseudobiogenic source in each case. Runs discussed in this section are summarized in Table 2.

Plate 1 shows the Pacific region data/model comparisons. The data set combines ship track measurements collected between 31°N and 61°S and annual mean mixing ratios from several locations (Hateruma, 24°N, 124°E; Okinawa, 27°N, 128°E; northwest Pacific cruise composite, 42°N–54°N [*Yokouchi et al.*, 2000], and the six long-term remote sites of *Khalil and Rasmussen* [1999]). It is not immediately obvious which simulation best matches the complete data set. The model results span the ship track data reasonably well at most locations, having a mean range of 40 pptv. The equatorial spike in the ship track data, which reflects local biomass burning and other emissions from Indonesia, is captured better when the pseudobiogenic emissions are more equatorially confined. Run 3800-w-coastal, which has strong local sources, shows an even higher equatorial spike (~1050 pptv), similar to spot measurements of 1000–2100 pptv on Java (6'S, omitted from the plate) [*Yokouchi et al.*, 2000]. However, run 3800-w-coastal also shows a stronger interhemispheric difference than either the ship track data or the other run results. Annual mean measurements at the remote long-term monitoring sites are best matched by runs 3800-w and 3900-h, which fall within 15 pptv of the data at each location (Figure 6). The major features of the seasonal cycles at the six long-term sites are well produced (Plate 2), and values simulated with the 3800 and 3900 Gg yr^{-1} net sources (red, purple, and green curves) generally fall within observational variability, while those from the 4000 Gg yr^{-1} (blue curves) and 4100 Gg yr^{-1} sources often exceed the range of measured values. This is also true at several short-term sites and leads us to prefer the lower net sources. The following sections discuss model sensitivity at various other measurement sites to the source distributions.

5.3.1. Effects of coastal versus inland emissions. Model results at Jaburu, in the Brazilian interior (Figure 7a), contradict our original assumption that all warm-climate green plants emit CH_3Cl in strict proportion to leaf area. Mixing ratios from run 3800-w exceed measurements [*Khalil and Rasmussen*, 1999] at Jaburu by 200–400 pptv. Reallocating the pseudobiogenic source

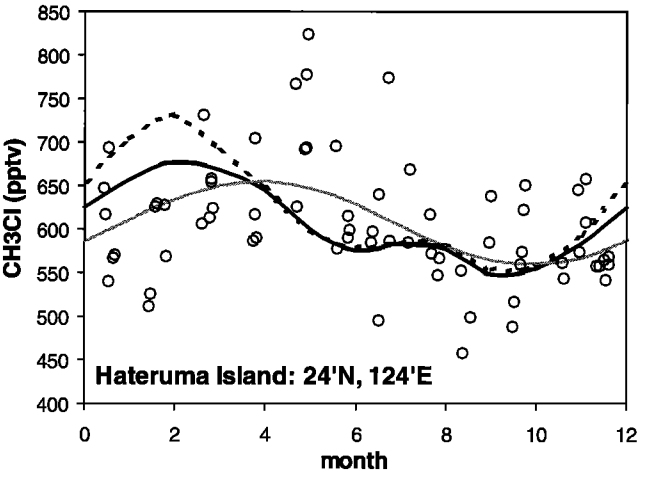

Figure 8. Sensitivity of model results to seasonality of pseudobiogenic source at Hateruma (24°N, 124°E). Solid curve indicates run 3880-h-seasonal, pseudobiogenic source varies according to monthly mean temperature; dotted curve indicates run 3880-h-invariant; shaded curve indicates published sinusoidal fit to the measurements [*Yokouchi et al.*, 2000]; circles indicate individual measurements.

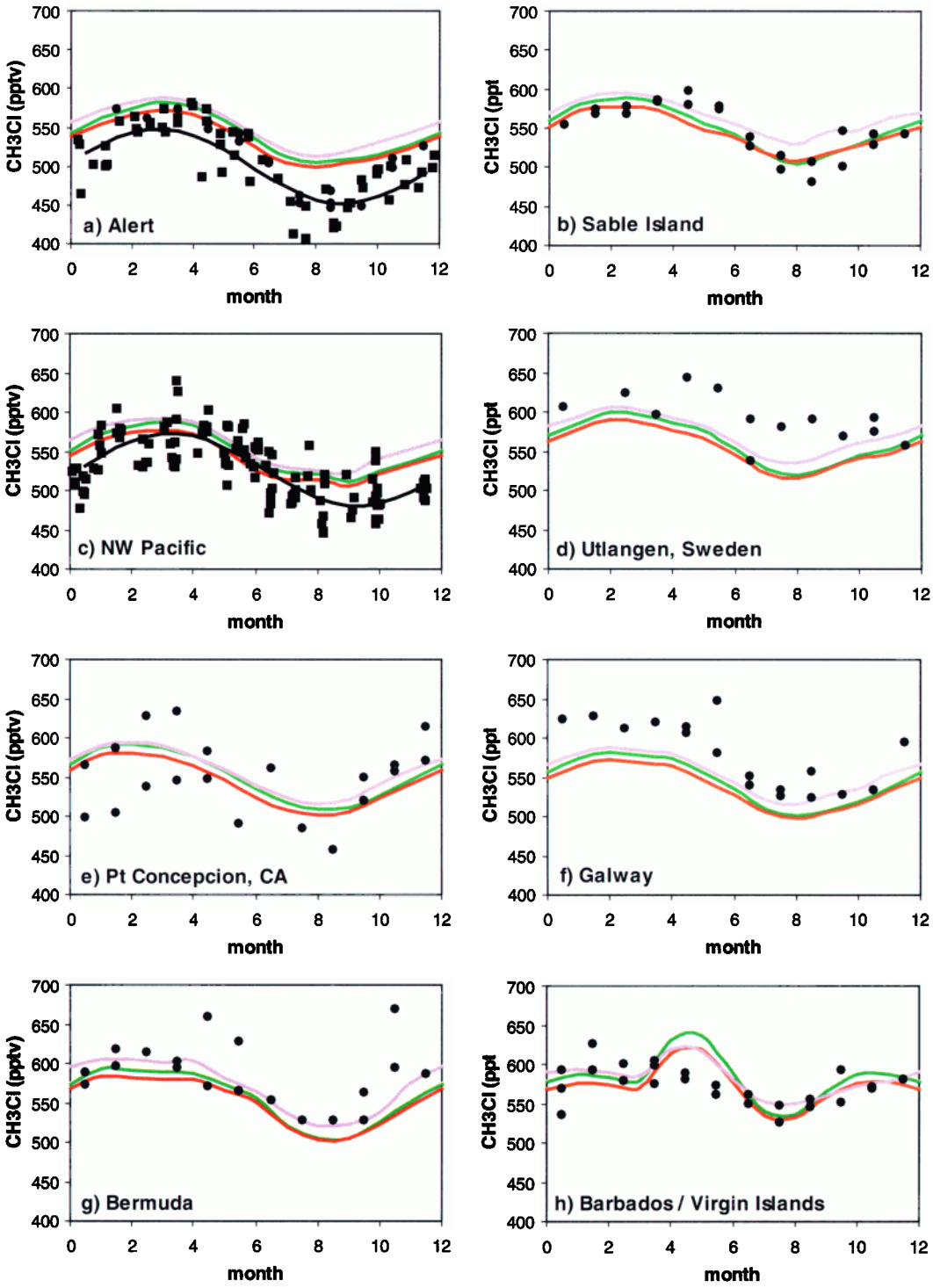

Plate 3. Comparisons of model results with observations at (a) Alert (82°N, 62°W); (b) Sable Island, Nova Scotia (44°N, 60°W); (c) northwestern Pacific cruise composite; (d) Utlangen, Sweden (56°N, 16°E); (e) Point Concepcion, California (34°N, 121°W); (f) Galway, Ireland (53°N, 9°W); (g) Bermuda (32°N, 64°W); and (h) Barbados (13°N, 59°W) and Virgin Islands (17°N, 63°W). Squares indicate data of *Yokouchi et al.* [2000]; circles indicate data of *Khalil and Rasmussen* [1999]. Black curves indicate sinusoidal data fits [*Yokouchi et al.*, 2000]; red curves indicate run 3800-w; green curves indicate run 3900-h; purple curves indicate run 3800-w-coast.

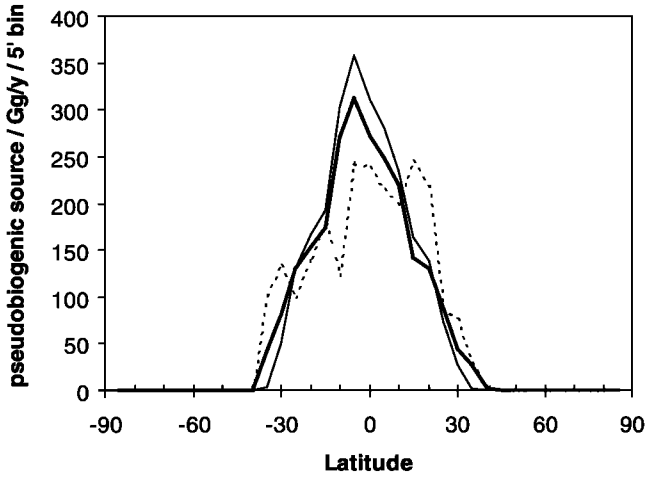

Figure 9. Pseudobiogenic source parameterizations, by 5° bins. Bold solid curve indicates run 3800-w; thin solid curve indicates run 3900-h; dotted curve indicates run 3800-w-coastal.

emissions to the 5° × 5° grid cells along the coast (run 3800-w-coastal, dotted curve in Figure 7a) allowed Jaburu mixing ratios to drop significantly, matching the measured values, without greatly affecting the modeled global burden. At Panama, modeled as an oceanic grid box influenced by nearby coastlines, mixing ratios were initially underestimated by 100–200 pptv (Figure 7b). Coastal pseudobiogenic emissions produced a mixing ratio increase at this location of up to 135 pptv, again better matching the observations. This result suggests that lower-latitude coastal and near-coastal emissions may be more important than currently supposed. If large inland sources do exist, they do not appear to significantly influence mixing ratios at Jaburu. These results do not contradict current midlatitude salt marsh flux estimates. Rather, they suggest that our global extrapolation of those fluxes is inadequate. It is possible that additional near-coastal sources of CH_3Cl exist at lower latitudes or that low-latitude coastal marshes give a much larger flux rate than the current parameterization allows. Similar deficiencies could be likely found in extrapolations of other fluxes to regions where representative measurements do not exist.

5.3.2. Effects of tropical source seasonality. Seasonality of the pseudobiogenic source was parameterized by varing emissions in response to monthly mean air temperature. Modeled monthly results at Hateruma Island (24°N, 124°E) show lower annual mean

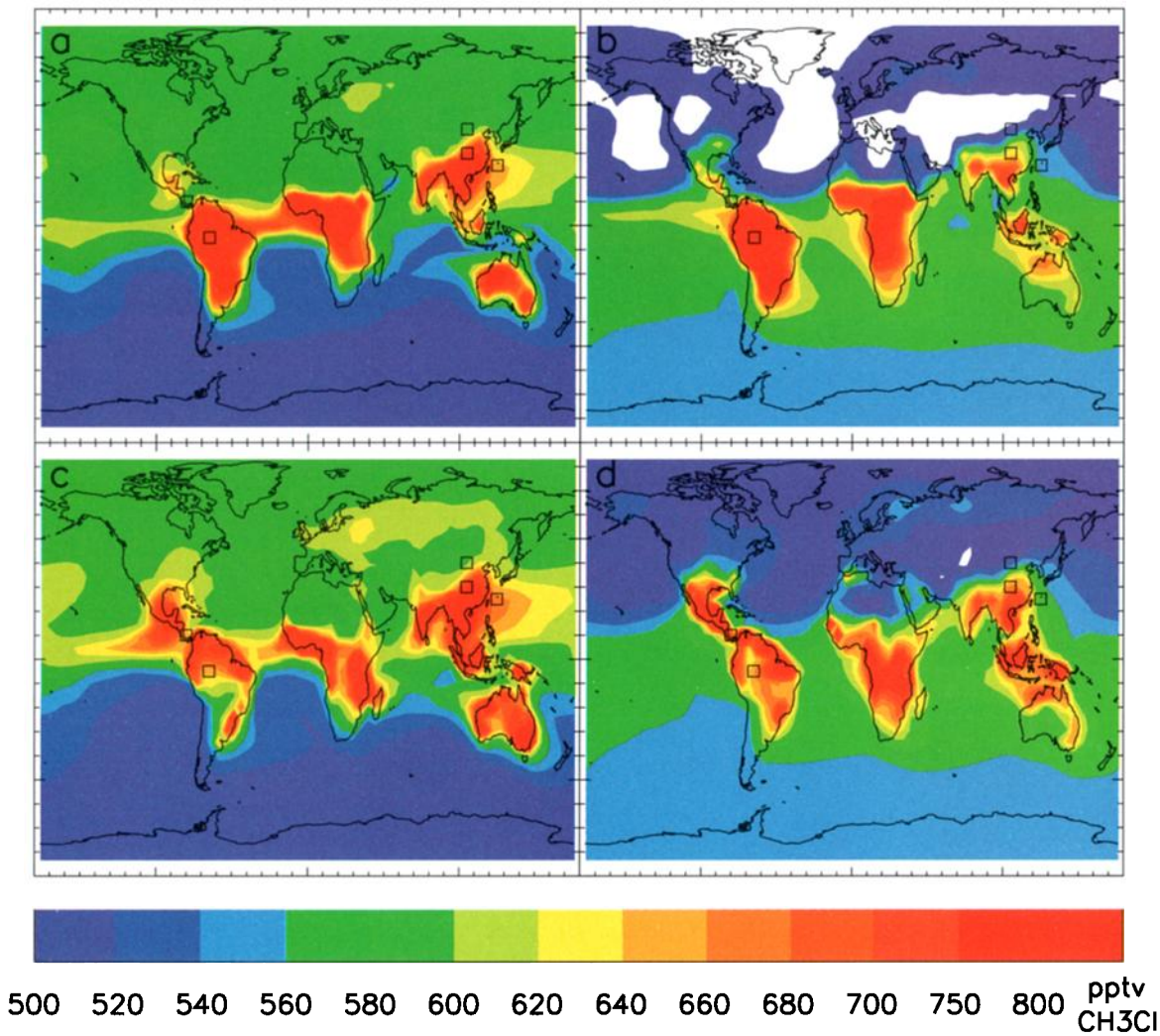

Plate 4. Surface mixing ratio results: (a) run 3800-w, February; (b) run 3800-w, August; (c) run 3800-w-coastal, February; and (d) run 3800-w-coastal, August. Contours are at a spacing of 20 pptv from 500 to 700 pptv and at 750 and 800 pptv. Open squares represent grid cells at (from left) Panama, Jaburu, Minqin, 8°S of Minqin, and Hateruma.

mixing ratios resulting from seasonal emissions (solid curve, Figure 8) than when the same net emissions are constant (dotted curve), since seasonality increases contributions from warmer, more equatorial latitudes, where CH_3Cl lifetimes are shorter, at the expense of cooler latitudes. The seasonal pseudobiogenic emissions case also shows a damping of the modeled seasonal cycle (by about 30% at Hateruma), owing to phase coincidence between emissions and OH-mediated CH_3Cl loss rates, which are also temperature-dependent. Seasonal cycle damping also occurred, albeit to a lesser extent, for some higher-latitude remote sites, such as Cape Grim, Cape Meares, and Barrow. (The paired sensitivity runs shown here did not include the salt marsh or wetland sources and are therefore not listed in Table 2 or used for assessment of global budget closure. Later results suggest that explicit representation of those sources has little effect on these conclusions.)

5.3.3. Results and sensitivity at other sites. Results for runs 3800-w, 3800-w-coastal, and 3900-h compare favorably with observations from other short-term monitoring stations in terms of both magnitude and seasonal variation (Plate 3). Agreement is especially good at Sable Island and at the stations around the Pacific and the Carribean. Mixing ratios are overpredicted by up to 50 pptv at Alert and underpredicted by a similar amount in northern Europe, likely due to biases in the model transport.

Run 3800-w-coastal gives slightly higher mixing ratios than the other two runs at all the extratropical Northern Hemisphere sites shown here, reflecting differences in the interhemispheric distributions of the pseudobiogenic source estimates. N/S ratios of this source were 0.79 and 0.80 for runs 3800-w and 3900-h, respectively, and 1.04 for run 3800-w-coastal (Figure 9 and Table 2).

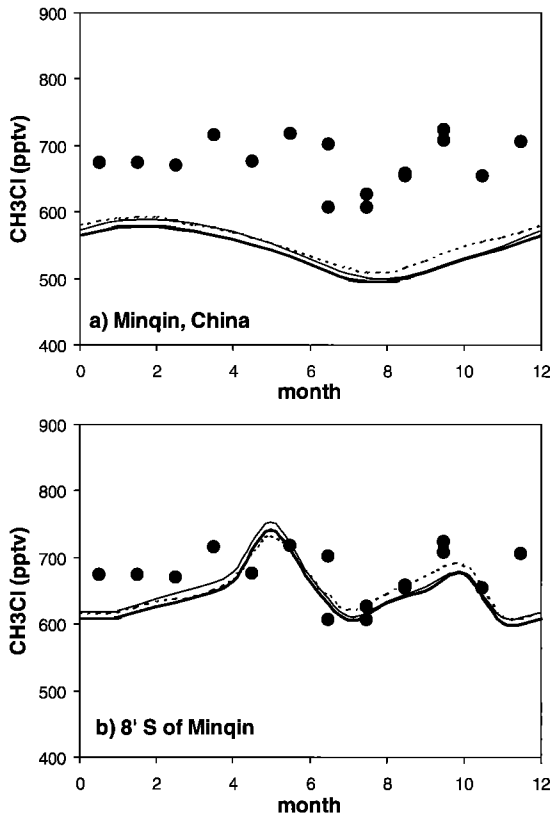

Figure 10. Model results at (a) Minqin, China (38°N, 103°E) and (b) grid cell centered 8°S of Minqin. Bold curves indicate run 3800-w; thin curves indicate run 3900-h; dotted curves indicate run 3800-w-coastal. Circles represent data of *Khalil and Rasmussen* [1999].

The lower N/S pseudobiogenic source ratios produce clean-air distributions that are more symmetrical about the equator and agree better with the measurements (Figure 6). This result supports a southern bias to the source, rather than provides evidence for preferring a particular source mechanism, since our additional source distributions are arbitrary. Most of the remote locations, especially those at higher latitudes, show relative insensitivity to other variations in pseudobiogenic source input.

5.3.4. The global budget. Our model best reproduces observed mixing ratios using a net surface source of 3800–3900 Gg yr^{-1}, which is about 12% greater than that derived by *Khalil and Rasmussen* [1999]. Our calculated global burden of about 4.8 Tg exceeds by 20% the 4.0 Tg (2.8 Tg Cl) quoted by *Keene et al.* [1999] (Table 2). In section 5.2 we demonstrated that the modeled global mean mixing ratio exceeds that derived from clean-air sites only, due to zonal mixing ratio inhomogeneities; the global burden is likewise affected. Plate 4 shows simulated mixing ratio distributions for February and August, months when strong interhemispheric gradients occur. Major source regions show elevated mixing ratios. The effects of downwind transport are also visible. Observations at some measurement sites of greatly elevated mixing ratios (e.g., Figure 7) show that zonal inhomogeneities are not merely a model artifact. At Minqin, China (38°N, 103°E) (Figure 10a), we underpredicted mixing ratios by 100–150 pptv. At most 40 pptv of this discrepancy can be attributed to our parameterized 50% reduction in Chinese biomass burning emissions. Results in the grid cell centered 8° (610–1170 km) farther to the south showed a much closer correspondence to observations (Figure 10b). The discrepancy likely reflects inadequacies in our modeled transport from the source regions, inadequacies in the source distributions, or unknown local sources. Minqin is located within the Asian interior, just upwind of a significant gradient in model mixing ratios (Plate 4). Model results from 5.5 km (not depicted) show that these gradients do not persist into the middle troposphere. Instead, the distribution at that altitude reflects transport of CH_3Cl away from the major source regions and mixing throughout the atmosphere.

6. Conclusions

We have presented a 3-D model study of the global tropospheric CH_3Cl budget and its imbalance. We showed (section 4) that the uncertainty in the OH + CH_3Cl reaction rate is not the major cause of the budget imbalance, as it cannot explain the interhemispheric distribution. We cannot preclude possible atmospheric production of CH_3Cl from sea-salt aerosol [*Keene et al.*, 1999]. However, our relative success in simulating inland, coastal, and clean-air observations using only a land-based (or coastal) additional source parameterization strengthens the case for the importance of terrestrial emissions.

We closed our model budget with a seasonally varying land-based source from the tropics and subtropics. Best model-data matches are obtained with pseudobiogenic sources of 2330–2430 Gg yr^{-1} (including 177 Gg yr^{-1} redistributed from Asian biomass burning emissions), with modeled net sources of 3800–3900 Gg y^{-1}, and a global burden of about 4.8 Tg CH_3Cl. Differences from previously published estimates are due to the 3-D representation of zonal mixing ratio inhomogeneities and to our finer spatial resolution of emissions and tropospheric loss processes.

Trace gas monitoring efforts traditionally use remote stations and "background" air to assess global abundances and large-scale budget balances. However, we found that CH_3Cl mixing ratios at most remote measurement sites are insensitive to the precise details of the tropical/subtropical source parameterization (i.e., degree of coastal enhancement, or precise latitudinal

extent), while tropical land-based sites such as Jaburu and Panama are more sensitive. We suggest that further constraining this source and its production mechanisms by means of models (i.e., 3-D inverse modeling studies) will be relatively difficult without more observations from sensitive locations. Specifically, there is little information regarding mixing ratios and seasonal cycles at locations within the tropics. Inland midlatitude observations would also be useful, to help define the latitudinal extent and nature of the additional source. Field studies are essential if the actual characteristics and mechanisms of CH_3Cl emissions are to be unequivocally identified. Flux characteristics and processes may well vary regionally in response to variations in vegetation type and species, soil type, sea-salt deposition, and local climate. Development of a global experimentally based flux distribution for the additional source of CH_3Cl therefore presents a major challenge, akin to that presented by the other major sources. Since so little is known at present, however, any new experimental information would be a major advance, especially if it could be incorporated into a global model of the CH_3Cl budget.

Acknowledgments. The National Center for Atmospheric Research is sponsored by the National Science Foundation. The authors are grateful to Sue Schauffler, Steve Montzka, and two anonymous reviewers, whose insightful comments greatly improved the paper. We also thank J. Lobert, D. Kinnison, and L. Emmons for helpful discussions.

References

Butler, J. H., M. Battle, M. L. Bender, S. A. Montzka, A. D. Clarke, E. S. Saltzman, C. M. Sucher, J. P. Severinghaus, and J. W. Elkins, A record of atmospheric halocarbons during the twentieth century from polar firn air, *Nature*, *399*, 749–755, 1999.

Chapman, V. J., Introduction, in *Ecosystems of the World, vol. 1, Wet Coastal Systems*, edited by V. J. Chapman, pp. 1– 30, Elsevier Sci., New York, 1997.

Cleveland, C. C., E. A. Holland, and J. C. Neff, Temperature regulation of soil respiration in an alpine tundra ecosystem, paper presented at the Front Range Branch Annual Meeting, Am. Geophys. Union, Golden, Colo., Feb. 8–10, 1993.

DeMore, W. B., S. P. Sander, D. M. Golden, R. F. Hampson, M. J. Kurylo, C. J. Howard, A. R. Ravishankara, C. E. Kolb, and M. J. Molina, Chemical kinetics and photochemical data for use in stratospheric modeling, *JPL Publ. 97-4, Eval. 12*, Jet Propul. Lab., Pasadena, Calif., 1997.

Dimmer, C. H., P. G. Simmonds, G. Nickless, and M. R. Bassford, Biogenic fluxes of halomethanes from Irish peatland ecosystems, *Atmos. Environ.*, *35*, 321–330, 2001.

Graedel, T. E., and W. C. Keene, Preface, *J. Geophys. Res.*, *104*, 8331–8332, 1999.

Granier, C., W.-M. Hao, G. Brasseur, and J.-F. Muller, Land use practices and biomass burning: Impact on the chemical composition of the atmosphere, in *Biomass Burning and Global Change*, vol. 1, edited by J. S. Levine, pp. 140– 148, MIT Press, Cambridge, Mass., 1996.

Guenther, A., et al., A global model of natural volatile organic compound emissions, *J. Geophys. Res.*, *100*, 8873–8892, 1995.

Guenther, A., B. Baugh, G. Brasseur, J. Greenberg, P. Harley, L. Klinger, D. Serça, and L. Vierling, Isoprene emission estimates and uncertainties for the central African EXPRESSO study domain, *J. Geophys. Res.*, *104*, 30,625–30,639, 1999.

Holland, E. A., A. R. Townsend, and P. M. Vitousek, Variability in temperature regulation of CO_2 fluxes and N mineralization from five Hawaiian soils: Implications for a changing climate, *Global Change Biol.*, *1*, 115–123, 1995.

Kalnay, E., et al., The NCEP/NCAR reanalysis project, *Bull. Am. Meteorol. Soc.*, *77*, 437– 471, 1996.

Keene, W. C., et al., Composite global emission of reactive chlorine from anthropogenic and natural sources: Reactive Chlorine Emissions Inventory J. Geophys. Res., *104*, 8429–8440, 1999.

Keppler, F., R. Eiden, V. Niedan, J. Pracht, and H. F. Schöler, Halocarbons produced by natural oxidation processes during degradation of organic matter, *Nature*, *403*, 298–301, 2000.

Khalil, M. A. K., Reactive chlorine compounds in the atmosphere, in *Reactive Halogen Compounds in the Atmosphere*, section 2, edited by P. Fabian and O. N. Singh, Springer-Verlag, New York, 1999.

Khalil, M. A. K., and R. A. Rasmussen, Atmospheric methyl chloride, *Atmos. Environ.*, *33*, 1305–1321, 1999.

Khalil, M. A. K., R. M. Moore, D. B. Harper, J. M. Lobert, D. J. Erickson, V. Koropalov, W. T. Sturges, and W. C. Keene, Natural emissions of chlorine-containing gases: Reactive Chlorine Emissions Inventory J. Geophys. Res., *104*, 8333–8345, 1999.

Kiehl, J. T., J. J. Hack, G. B. Bonan, B. A. Boville, B. P. Briegleb, D. L. Williamson, and P. J. Rasch, Description of the NCAR Community Climate Model (CCM3), *NCAR Tech. Note 420+STR*, Natl. Cent. for Atmos. Res., Boulder, Colo., 1996.

Koppmann, R., F. J. Johnen, C. Plass-Dülmer, and J. Rudolph, Distribution of methyl chloride, dichloromethane, trichloroethene, and tetrachloroethene over the North and South Atlantic, *J. Geophys. Res.*, *98*, 20,517–20,526, 1993.

Kurylo, M. J., et al., Short-lived ozone-related compounds, in *Scientific Assessment of Ozone Depletion: 1998*, edited by D. L. Albritton et al., pp. 2.1–2.56, WMO Global Ozone Res. and Monit. Proj., *Rep. 44*, World Meteorol. Organ., Geneva, Switzerland, 1999.

Lee-Taylor, J. M., and E. A. Holland, Litter decomposition as a potential natural source of methyl bromide, *J. Geophys. Res.*, *105*, 8857–8864, 2000.

Lee-Taylor, J. M., S. C. Doney, G. P. Brasseur, and J.-F. Müller, A global three-dimensional atmosphere-ocean model of methyl bromide distributions, *J. Geophys. Res.*, *103*, 16,039–16,059, 1998.

Lobert, J. M., W. C. Keene, J. A. Logan, and R. Yevich, Global chlorine emissions from biomass burning: Reactive Chlorine Emissions Inventory J. Geophys. Res., *104*, 8373–8389, 1999.

Manö, S., and M. O. Andreae, Emission of methyl bromide from biomass burning, *Science*, *263*, 1255–1257, 1994.

Matthews, E., Global vegetation and land use: New high-resolution databases for climate studies, *J. Clim. Appl. Meteorol.*, *22*, 474–486, 1983.

Matthews, E., Global litter production, pools, and turnover times: Estimates from measurement data and regression models, *J. Geophys. Res.*, *102*, 18,771–18,800, 1997.

Matthews, E., and I. Fung, Methane emission from natural wetlands: Global distribution, area, and environmental characteristics of sources, *Global Biogeochem. Cycles*, *1*, 61–86, 1987.

McCulloch, A., M. L. Aucott, C. M. Benkovitz, T. E. Graedel, G. Kleiman, P. Midgley, and Y. F. Li, Global emissions of hydrogen chloride and chloromethane from coal combustion, incineration, and industrial activities: Reactive Chlorine Emissions Inventory, *J. Geophys Res*, *104*, 8391–8403, 1999.

Montzka, S. A., J. H. Butler, J. W. Elkins, T. M. Thompson, A. D. Clarke, and L. T. Lock, Present and future trends in the atmospheric burden of ozone-depleting halogens, *Nature*, *398*, 690–694, 1999a.

Montzka, S. A., J. H. Butler, J. W. Elkins, L. Lock, and D. Mondeel, Seasonal and interannual variability of methyl bromide and methyl chloride from a global flask sampling network, *Eos Trans. AGU*, *80*(46), Fall Meet. Suppl., F149, 1999b.

Moore, R. M., W. Groszko, and S. J. Niven, Ocean-atmosphere exchange of methyl chloride: Results from NW Atlantic and Pacific Ocean studies, *J. Geophys. Res.*, *101*, 28,529–28,538, 1996.

Müller, J.-F., Geographical distribution and seasonal variation of surface emissions and deposition velocities of atmospheric trace gases, *J. Geophys. Res.*, *97*, 3787–3804, 1992.

Müller, J.-F., and G. Brasseur, IMAGES: A three-dimensional chemical transport model of the global atmosphere, *J. Geophys. Res.*, *100*, 16,445–16,490, 1995.

Prinn, R. G., R. F. Weiss, B. R. Miller, J. Huang, F. N. Alyea, D. M. Cunnold, P. J. Fraser, D. E. Hartley, and P. G. Simmonds, Atmospheric trends and lifetime of CH_3CCl_3 and global OH concentrations, *Science*, *269*, 187–192, 1995.

Redeker, K. R., N.-Y. Wang, J. C. Low, M. McMillan, S. C. Tyler, and R. J. Cicerone, Emissons of methyl halides and methane from rice paddies, *Science*, *290*, 966–969, 2000.

Rhew, R. C., B. R. Miller, and R. F. Weiss, Natural methyl bromide and methyl chloride emissions from coastal salt marshes, *Nature*, *403*, 292–295, 2000.

Schauffler, S. M., L. E. Heidt, W. H. Pollock, T. M. Gilpin, J. F. Vedder, S. Solomon, R. A. Lueb, and E. L. Atlas, Measurements of halogenated organic compounds near the tropical tropopause, *Geophys. Res. Lett.*,*22*, 2567–2570, 1993.

Shea, D. J., K. E. Trenberth, and R. W. Reynolds, A global monthly seasurface temperature climatology, *NCAR Tech. Note NCAR/TN-345+STR*, 167 pp., Natl. Cent. for Atmos. Res., Boulder, Colo., 1990.

Shea, D. J., K. E. Trenberth, and R. W. Reynolds, A global monthly sea surface temperature climatology, *J. Clim.*, *5*, 987–1001, 1992.

Shorter, J. H., C. E. Kolb, P. M. Crill, R. A. Kerwin, R. W. Talbot, M. E. Hines, and R. C. Harriss, Rapid degradation of atmospheric methyl bromide in soils, *Nature*, *377*, 717–719, 1995.

Spivakovsky, C.M., et al., Three-dimensional climatological distribution of

tropospheric OH: Update and evaluation, *J. Geophys. Res.*, *105*, 8931–8980, 2000.

Varner, R. K., P. M. Crill, and R. W. Talbot, Wetlands: A potentially significant source of atmospheric methyl bromide and methyl chloride, *Geophys. Res. Lett.*, *26*, 2433–2436, 1999.

Varner, R. K., P. M. Crill, R. W. Talbot, C. H. Mosedale, and M. L. White, Seasonal exchange of methyl bromide at fresh and saltwater wetlands, *Eos Trans. AGU*, *81*(48), Fall Meet. Suppl., F264, 2000.

Wanninkhof, R., Relationship between wind speed and gas exchange over the ocean, *J Geophys Res.*, *97*, 7373–7382, 1992.

Watling, R., and D. B. Harper, Chloromethane production by wood-rotting fungi and an estimate of the global flux to the atmosphere, *Mycol. Res.*, *102*, 769–787, 1998.

Yokouchi, Y., Y. Nojiri, L. A. Barrie, D. Toom-Sauntry, T. Machida, Y. Inuzka, H. Akimoto, H.-J. Li, Y. Fujinuma, and S. Aoki, A strong source of methyl chloride to the atmosphere from tropical coastal land, *Nature*, *403*, 295–298, 2000.

G. P. Brasseur, Max Planck Institute for Meteorology, Bundestrasse 55, 20146 Hamburg, Germany.

J. M. Lee-Taylor, NCAR Atmospheric Chemistry Division, 1850 Table Mesa Drive, Boulder, CO 80303, USA. (julial@ucar.edu)

Y. Yokouchi, National Institute for Environmental Studies, 16-2 Onogawa, Tsukuba, Ibaraki 305-0053, Japan.

(Received September 7, 2000; revised March 9, 2001;
accepted April 13, 2001.)